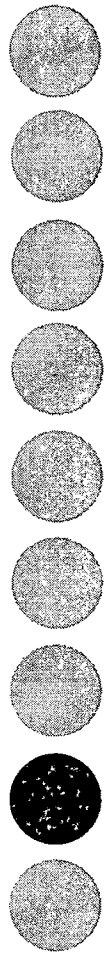


*In Vivo Studies*



## 8.1 BIODISTRIBUTION STUDY

### 8.1.1 Materials

Sodium pertechnetate (Tc-99m) freshly eluted from 99Mo by solvent extraction method was procured from the Regional Center for Radiopharmaceuticals, Board of Radiation and Isotope Technology (BRIT), Department of Atomic Energy, India. Stannous chloride dehydrate ( $\text{SnCl}_2 \cdot 2\text{H}_2\text{O}$ ) was purchased from Sigma Aldrich, Mumbai. Instant thin layer chromatography (ITLC) plates were purchased from Gelman Science Inc (Ann Arbor, MI).

### 8.1.2 Animals

Balb/C mice of age group between 6-8 weeks were used for biodistribution studies. The animals were maintained in a room ( $23 \pm 2$  °C and  $60 \pm 10$  % humidity) under 12 h light/dark cycle. Food and water were given *ad libitum*. All animal studies were carried out under the guidelines compiled by Committee for the Purpose of Control and Supervision of Experiments on Animals, Ministry of Culture, Government of India (CPCSEA), and all the study protocols were approved by the Animal Ethics Committee of the INMAS, New Delhi.

### 8.1.3 Radiolabeling of ETO and micellar formulations

ETO and ETO loaded micellar formulations were radiolabeled with Technetium-99m ( $^{99\text{m}}\text{Tc}$ ) by direct labeling method using  $\text{SnCl}_2 \cdot 2\text{H}_2\text{O}$  as the reducing agents as reported earlier (Snehalatha et al., 2008). Briefly, 1 ml of ETO solution and ETO loaded micellar formulations (equivalent to 1 mg/ml of ETO) were individually mixed with 50  $\mu\text{l}$  of  $\text{SnCl}_2 \cdot 2\text{H}_2\text{O}$  (2 mg/ml) and the pH of formulations was adjusted to 6.5 with 0.5 M sodium bicarbonate solution. Then, 0.1 ml of freshly eluted Tc-99m pertechnetate solution (2 mCi) was added to each preparation, mixed well, and incubated for 15 min at room temperature. Final radioactivity present in the preparation was checked using dose calibrator (Gamma ray scintillation counter, Capintec, CAPRAC-R). The effect of the amount of  $\text{SnCl}_2 \cdot 2\text{H}_2\text{O}$  on radiolabeling efficacy was optimized based on quality control tests for the labeled complex as described earlier (Theobald, 1990).

#### 8.1.4 Determination of labeling efficiency

The labeling efficiency of ETO and ETO loaded micellar formulations were performed as reported earlier (Babbar et al., 1991) by developing ascending thin layer chromatography (TLC) using instant thin-layer chromatography strips coated with silica gel (ITLCSG). ITLC strips were used to determine free technetium and percentage of radio colloids in the preparation. Based on these two parameters, the labeling efficiency of the preparation was calculated (Mishra et al., 1991).

ITLC strips were spotted with tiny drop (2-3  $\mu$ l) of radiolabeled formulations at 1 cm from one end and developed using acetone as mobile phase. The solvent front was allowed to reach up to a height of approximately 6 to 8 cm from the origin and the strip was cut horizontally into two halves. Radioactivity in each half was determined by well-type gamma ray spectrometer (Gamma ray scintillation counter, Capintec, CAPRAC-R). The free pertechnetate present in the preparation migrates to the top portion ( $R_f$  value = 0.9-1.0) of the ITLC strip, while radiolabeled formulations along with the radio colloids (reduced/hydrolyzed technetium) remained at the point of application. The presence of radio colloids was determined by developing ITLC strip using pyridine: acetic acid: water in ratio of 3:5:1.5. Reduced/hydrolyzed Tc- 99m present in the preparation will remain at the point of application, while both the free Tc-99m-pertechnetate as well as labeled complex migrates with the solvent front. By subtracting the migrated activity with the solvent front using acetone from that using pyridine: acetic acid: water mixtures, the net amount of  $^{99m}\text{Tc}$ -ETO or  $^{99m}\text{Tc}$ -ETO loaded micelles were calculated.

#### 8.1.5 *In vitro* stability of labeled complexes

Stability of the  $^{99m}\text{Tc}$  labeled complexes of ETO and ETO loaded micellar formulations was determined *invitro* in normal saline by ascending TLC technique. The labeled complex (0.1 ml) was incubated with normal saline (0.4 ml) at 37 °C up to 24 h. The samples were withdrawn at regular intervals up to 24 h and spotted on ITLCSG paper and TLC was performed as reported above. These strips were counted for radioactivity in gamma ray spectrometer and percentage labeling efficiency at different time interval was calculated for ETO and micellar formulations.

### 8.1.6 Tumor implantation

Ehrlich ascites tumor (EAT) cells were grown in the ascites fluid of mice by injecting  $1 \times 10^7$  cells intraperitoneally. The cells in exponential state were harvested and  $1.8 \times 10^6$  cells per mouse was injected subcutaneously in thigh of the right hind leg. After 8-10 days, a palpable tumor in the volume range of  $0.9 \pm 0.1 \text{ cm}^3$  was observed and used for further studies.

### 8.1.7 Biodistribution study

Biodistribution study of  $^{99m}\text{Tc}$  labeled ETO and ETO loaded micellar formulations (0.2 mg (ETO)/0.1 ml) was studied in EAT tumor bearing mice (Snehalatha et al., 2008; Yadav et al., 2008). The mice were divided into seven groups of 20 animals each (total 140 mice; five mice per formulation per time point). All animals were fasted overnight before the experiment but allowed free access to water *ad libitum*. Each mouse injected a 100  $\mu\text{Ci}$  (100  $\mu\text{l}$ ) dose of the labeled formulations (plain ETO and ETO loaded micelles) by intravenous route through tail vein. The mice were humanly killed by cervical dislocation at 1 h, 2 h, 4 h and 24 h post-injection. At these time intervals, the blood was collected by cardiac puncture and animals were sacrificed and the organs such as heart, lung, liver, kidney, spleen, stomach, intestine and tumor were isolated. All organs/tissue collected were washed thoroughly with Ringer's solution, dried using tissue paper and were taken in pre weighed tubes that were weighed again to calculate the weight of the organ/tissue. The radioactivity was measured using well-type gamma scintillation counter (Gamma ray scintillation counter, Capintec, CAPRAC-R) along with three aliquots of the diluted standard representing 100 % of injected radioactivity. The results were expressed as percentage of injected dose (ID) per gram of an organ.

## 8.2 EXPERIMENTAL METASTASIS STUDY

### 8.2.1 Animals

Experimental metastasis study was performed using pathogen free female C57BL/6 mice of age 6-8 weeks procured from Animal house, Advanced Centre for Treatment, Research and Education in Cancer (ACTREC), Navi Mumbai. All animal studies were carried out under the guidelines compiled by Committee for the Purpose of

Control and Supervision of Experiments on Animals, Ministry of Culture, Government of India (CPCSEA), and all the study protocols were approved by the Institutional Animal Ethics Committee of the ACTREC, Navi Mumbai. The animals were maintained in a room ( $23 \pm 2^\circ\text{C}$  and  $60 \pm 10\%$  humidity) under 12 h light/dark cycle. Food and water were given *ad libitum*.

### **8.2.2 *In vitro* treatment of B16F10 melanoma cells with formulations and its effect on inhibition of lung metastasis (Pre-treatment method)**

The *in vitro* drug treated B16F10 cell induced metastasis was performed as reported earlier (Gude et al., 1996, Ratheesh et al., 2007). The B16F10 cells were seeded in to 60 mm tissue culture plates at cell density of  $2 \times 10^4$  cells/ml in complete media. On next day, cells were treated with plain ETO and ETO loaded micellar formulations prepared in complete media at subtoxic dose (half  $\text{IC}_{50}$  value, 48 h) and incubated for 48 h at  $37^\circ\text{C}$ . Cells were washed with PBS twice and harvested using saline EDTA and final count of cells was made to  $1 \times 10^6$  cells/ml in PBS. The drug treated cells were inoculated ( $1 \times 10^5$  cells/0.1 ml of PBS) to C57BL/6 mice via tail vein. The mice were randomly assigned to eight group (5 mice/group) in which one group was assigned as control which received untreated B16F10 cells. All mice were sacrificed on day 21<sup>st</sup> day of cell inoculation by cervical dislocation, their lungs excised and the number of pulmonary metastatic nodules (lung colonies) on the surface was counted under a dissecting microscope. The percent inhibition in formation of pulmonary metastatic nodules in mice due to inoculation of ETO and micellar formulations treated B16F10 cells was calculated with respect to the number of nodules present in the untreated control group.

### **8.2.3 *In vivo* treatment of B16F10 melanoma and its effect on inhibition of lung metastasis with formulations (Post-treatment method)**

C57BL/6 mice were injected with 0.1 million B16F10 cells in 0.1 ml of PBS through intravenous route by tail vein (Sant et al., 2000, Gude et al., 1999). Mice were randomly assigned to eight groups (5 mice/group) in which one group were assigned as control which received only B16F10 cells. On next day of cell inoculation, plain ETO and ETO loaded micellar formulations were injected at dose of drug 2 mg/kg intravenously by tail vein. The animals were sacrificed by cervical dislocation on 21<sup>st</sup>

day of cell inoculation and lungs were excised. The further procedure followed was similar as reported above in section 8.2.2.

#### **8.2.4 Histopathology study**

After counting pulmonary metastatic nodules, lungs were fixed in 10 % buffered formaldehyde. The tissue was processed through a histological routine with a Shandon Pathcentre Tissue Processor. Paraffin sections were cut at 5  $\mu\text{m}$  thickness, stained with haematoxylin and eosin to study tissue morphology. Microscopic images were taken using Zeiss AxioImager Z-1 (Germany) microscope.

### **8.3 RESULTS AND DISCUSSION**

#### **8.3.1 Biodistribution study**

##### **8.3.1.1 Radiolabeling efficiency of ETO and micellar formulations**

In this study,  $^{99\text{m}}\text{TcO}_4^-$  (Technetium-99m) was used as radiolabeling compound because of easy availability, cost-effectiveness, and low radiation dose. Since the half-life of  $^{99\text{m}}\text{TcO}_4^-$  is 6 h when compared with 60 days for  $^{125}\text{I}$ , it presents less radiation burden.  $^{99\text{m}}\text{Tc}$  has been used to directly label preformed nanoparticles using  $\text{SnCl}_2$  as a reducing agent (Yadav et al., 2008). Chemically,  $^{99\text{m}}\text{TcO}_4^-$  is a non-reactive species and does not label any compound by direct addition. In  $^{99\text{m}}\text{Tc}$  labeling of many compounds, prior reduction of  $^{99\text{m}}\text{TcO}_4^-$  from the 7 + state to a lower oxidation state (4+) is required and was achieved using  $\text{SnCl}_2 \cdot 2\text{H}_2\text{O}$  and pH was adjusted to 6.5 before addition of ETO and micellar formulations. The effect of pH on radiolabeling was well reported by Halder et al. (2008). They observed that at pH 6.5, maximum labeling with minimum amount of free and radiocolloid formation occurred. Incubation time of 15 min gave maximum labeling as per previous report and was kept 15 min in present studies (Halder et al., 2008). The amount of stannous chloride used for reducing the pertechnetate played an important role in the labeling process. Lower amounts of  $\text{SnCl}_2 \cdot 2\text{H}_2\text{O}$  led to poor labeling efficiency while higher amounts led to the greater formation of undesirable radiocolloids (Reddy et al., 2005). Table 8.1 to 8.3 represents the influence of  $\text{SnCl}_2 \cdot 2\text{H}_2\text{O}$  on labeling efficiency and formation of radiocolloids. The optimum amount of  $\text{SnCl}_2 \cdot 2\text{H}_2\text{O}$  required for high labeling efficiency with least formation of radiocolloids was found to be 75  $\mu\text{g}$  for ETO and 100  $\mu\text{g}$  for micellar formulations.

SnCl <sub>2</sub> ·2H <sub>2</sub> O O (µg)	ETO		
	% labeled	% colloids	% free
25	78.89 ± 1.58	1.86 ± 0.06	19.25 ± 1.70
50	87.79 ± 1.94	1.62 ± 0.09	10.59 ± 1.65
75	98.08 ± 1.67	0.64 ± 0.08	1.28 ± 0.29
100	90.21 ± 1.01	8.18 ± 2.07	1.61 ± 0.82
150	80.92 ± 0.76	17.56 ± 3.20	1.52 ± 0.73

**Table 8.1 Influence of the amount of SnCl<sub>2</sub>·2H<sub>2</sub>O on the labeling efficiency of free ETO (Values are mean ± S.D. of three individual experiments)**

### 8.3.1.2 *In vitro* stability of labeled complexes

The *in vitro* stability studies of radiolabeled complex were carried out in normal saline upto 24 h and the results obtained are represented in Table 8.4 and 8.5. It was observed that all formulations were remained stable for 24 h of incubation and the change in percent labeling observed was negligible compared to initial data. The stability of the labeled complexes in normal saline indicates the usefulness of the label as a marker for the biodistribution studies.

SnCl <sub>2</sub> ·2H <sub>2</sub> O (µg)	MPCL235			YPCL235			EPCL235		
	% Labeled	% Colloids	% Free	% Labeled	% Colloids	% Free	% Labeled	% Colloids	% Free
	25	74.49 ± 1.11	0.56 ± 0.09	24.95 ± 1.56	75.10 ± 1.22	0.60 ± 0.10	24.3 ± 2.00	74.53 ± 1.80	0.63 ± 0.12
50	81.90 ± 1.65	0.76 ± 0.12	17.34 ± 2.10	82.60 ± 1.99	0.73 ± 0.15	16.67 ± 1.75	82.54 ± 2.18	0.72 ± 0.21	16.74 ± 0.95
75	89.04 ± 1.63	0.85 ± 0.25	10.11 ± 1.35	88.53 ± 2.15	0.95 ± 0.14	10.52 ± 1.04	86.17 ± 2.13	0.90 ± 0.14	12.93 ± 1.20
100	97.21 ± 1.21	1.45 ± 0.20	1.34 ± 0.09	96.30 ± 1.29	1.23 ± 0.36	2.41 ± 0.17	97.92 ± 0.92	1.17 ± 0.54	1.16 ± 0.15
150	89.23 ± 1.66	8.08 ± 1.79	2.69 ± 0.18	89.09 ± 1.42	9.64 ± 0.89	1.27 ± 0.12	90.32 ± 1.15	8.23 ± 1.47	1.45 ± 0.08

Table 8.2 Influence of amount of stannous chloride on the labeling efficiency of MPCL235, YPCL235 and EPCL235 micelles (Values are mean ± S.D. of three individual experiments)

SnCl <sub>2</sub> ·2H <sub>2</sub> O (µg)	MPCL570			YPCL570			EPCL570		
	% Labeled	% Colloids	% Free	% Labeled	% Colloids	% Free	% Labeled	% Colloids	% Free
	25	75.23 ± 1.58	0.63 ± 0.12	24.14 ± 2.09	72.98 ± 1.90	0.69 ± 0.08	26.33 ± 3.78	74.23 ± 2.23	0.76 ± 0.08
50	80.26 ± 1.84	0.72 ± 0.21	19.02 ± 3.56	78.98 ± 2.32	0.84 ± 0.09	20.18 ± 3.00	81.66 ± 1.46	0.88 ± 0.10	17.46 ± 1.52
75	85.98 ± 1.02	0.95 ± 0.07	13.07 ± 1.54	86.43 ± 1.98	0.90 ± 0.07	12.67 ± 2.32	87.83 ± 1.27	1.05 ± 0.20	11.12 ± 1.01
100	97.23 ± 1.34	1.11 ± 0.08	1.66 ± 0.04	97.66 ± 1.00	1.63 ± 0.07	0.71 ± 0.07	96.90 ± 1.45	1.70 ± 0.15	1.40 ± 0.43
150	89.92 ± 1.58	10.25 ± 1.02	0.17 ± 0.03	90.54 ± 1.82	8.45 ± 1.12	1.01 ± 0.04	90.58 ± 1.38	8.77 ± 1.44	0.65 ± 0.12

Table 8.3 Influence of amount of stannous chloride on the labeling efficiency of MPCL570, YPCL570 and EPCL570 micelles (Values are mean ± S.D. of three individual experiments)

Time (h)	% Radiolabeling			
	ETO	MPCL235	YPCL235	EPCL235
Initial	99.18 ± 1.67	98.11 ± 1.20	97.20 ± 1.39	98.12 ± 1.01
0.5	99.16 ± 1.35	98.23 ± 2.45	97.22 ± 1.88	98.01 ± 1.35
1	99.04 ± 1.42	98.15 ± 1.64	97.17 ± 1.92	97.80 ± 1.85
2	99.06 ± 1.35	98.10 ± 1.22	97.01 ± 1.77	97.76 ± 2.35
4	98.17 ± 2.67	98.02 ± 2.08	96.47 ± 1.63	97.61 ± 1.77
8	98.09 ± 1.47	98.04 ± 1.68	96.51 ± 1.98	97.77 ± 1.51
24	98.12 ± 1.91	97.99 ± 1.57	96.50 ± 2.12	97.69 ± 1.08

**Table 8.4 Stability of  $^{99m}\text{Tc}$  labeled ETO, MPCL235, YPCL235 and EPCL235 micelles in normal saline (Values are mean ± S. D. of three individual experiments)**

Time (h)	% Radiolabeling		
	MPCL570	YPCL570	EPCL570
Initial	98.43 ± 1.22	98.56 ± 2.27	98.98 ± 1.60
0.5	98.39 ± 1.41	99.01 ± 1.22	98.26 ± 1.87
1	98.45 ± 1.35	98.49 ± 1.33	98.34 ± 1.40
2	98.33 ± 1.63	98.32 ± 1.47	97.78 ± 1.23
4	98.20 ± 1.25	98.36 ± 1.60	98.12 ± 2.01
8	98.14 ± 1.98	98.13 ± 2.08	98.23 ± 1.33
24	98.16 ± 2.03	98.22 ± 1.42	98.05 ± 2.56

**Table 8.5 Stability of  $^{99m}\text{Tc}$  labeled etoposide, MPCL570, YPCL570 and EPCL570 micelles in normal saline (Values are mean ± S. D. of three individual experiments)**

### 8.3.1.3 Biodistribution study

The biodistribution study of  $^{99m}\text{Tc}$  labeled ETO and micellar formulations were performed after intravenous injection to EAT tumor bearing mice model. It is believed that compare to normal animal, the biodistribution pattern in tumor bearing animal will be different. The probable reason behind these might be due to the EPR (enhance permeation and retention) effect and receptor based endocytosis which results in to

higher tumor uptake of nanoparticles by means of passive and active targeting respectively. The most important criteria for radiolabeled complexes are their *in vivo* stability and the complex should not break down in the body after injection. This *in vivo* stability can be assessed by measuring radioactivity of labeled complex in stomach. It is reported that if the complex is not stable, the dissociated free  $^{99m}\text{Tc}$  accumulates at elevated level in stomach resulting in to greater radioactivity (Taylor et al., 1986). In the present study, as shown in Table 8.6 to 8.12, the stomach showed very less radioactivity ( $\leq 1\%$ ) in all the formulations, implies that the labeled complex was stable and results obtained were in accordance with earlier study carried out (Reddy et al., 2005).

Organs	% Injected dose per gram of tissue			
	1 h	2 h	4 h	24 h
Blood	1.32 ± 0.21	0.89 ± 0.25	0.55 ± 0.11	0.29 ± 0.05
Heart	1.96 ± 0.20	0.91 ± 0.06	0.57 ± 0.08	0.29 ± 0.03
Lung	4.36 ± 0.35	3.76 ± 0.20	2.92 ± 0.65	1.03 ± 0.10
Liver	7.96 ± 1.68	5.69 ± 1.04	4.16 ± 0.59	2.87 ± 0.17
Spleen	7.25 ± 0.68	5.70 ± 0.68	4.62 ± 0.22	2.05 ± 0.06
Kidney	6.63 ± 0.86	6.47 ± 0.98	4.95 ± 0.31	3.43 ± 0.05
Stomach	0.31 ± 0.08	0.26 ± 0.04	0.23 ± 0.10	0.15 ± 0.02
Intestine	0.51 ± 0.07	0.43 ± 0.06	0.35 ± 0.07	0.21 ± 0.02
Tumor	0.38 ± 0.07	0.26 ± 0.04	0.21 ± 0.02	0.08 ± 0.01

**Table 8.6 Biodistribution of  $^{99m}\text{Tc}$ -labeled ETO after intravenous injection in EAT bearing Balb/c mice. Radioactivity was counted in each organ and expressed as percent injected dose per gm of organ/tissue. Each value is the mean ± S. D. of 5 mice.**



Organs	% Injected dose per gram of tissue			
	1 h	2 h	4 h	24 h
Blood	3.90 ± 0.12	3.75 ± 0.54	3.44 ± 0.33	1.27 ± 0.14
Heart	1.14 ± 0.08	0.76 ± 0.11	0.52 ± 0.04	0.31 ± 0.13
Lung	2.25 ± 0.14	2.01 ± 0.35	1.31 ± 0.10	0.67 ± 0.02
Liver	12.07 ± 2.03	10.69 ± 1.83	7.52 ± 1.18	4.05 ± 0.69
Spleen	2.93 ± 0.10	2.61 ± 0.23	2.07 ± 0.08	0.98 ± 0.06
Kidney	3.67 ± 0.18	3.45 ± 0.28	2.61 ± 0.31	1.25 ± 0.07
Stomach	0.46 ± 0.05	0.37 ± 0.05	0.44 ± 0.04	0.11 ± 0.03
Intestine	0.83 ± 0.08	0.76 ± 0.08	0.58 ± 0.07	0.18 ± 0.08
Tumor	2.06 ± 0.14	2.64 ± 0.26	2.96 ± 0.17	1.67 ± 0.07

**Table 8.9** Biodistribution of  $^{99m}\text{Tc}$ -labeled EPCL235 after intravenous injection in EAT bearing Balb/c mice. Radioactivity was counted in each organ and expressed as percent injected dose per gm of organ/tissue. Each value is the mean  $\pm$  S. D. of 5 mice.

Organs	% Injected dose per gram of tissue			
	1 h	2 h	4 h	24 h
Blood	3.61 ± 0.27	3.44 ± 0.58	3.06 ± 0.41	1.14 ± 0.07
Heart	0.83 ± 0.04	0.74 ± 0.15	0.42 ± 0.07	0.25 ± 0.04
Lung	2.24 ± 0.10	2.06 ± 0.34	1.55 ± 0.24	0.87 ± 0.06
Liver	14.85 ± 2.38	9.37 ± 1.02	7.48 ± 1.30	3.18 ± 0.64
Spleen	4.52 ± 0.97	3.67 ± 0.28	2.83 ± 0.35	1.58 ± 0.20
Kidney	2.69 ± 0.27	3.54 ± 0.47	3.76 ± 0.22	1.65 ± 0.10
Stomach	0.24 ± 0.02	0.63 ± 0.08	0.42 ± 0.07	0.32 ± 0.05
Intestine	0.57 ± 0.06	0.48 ± 0.10	0.42 ± 0.09	0.16 ± 0.04
Tumor	0.82 ± 0.04	1.63 ± 0.12	1.92 ± 0.38	0.61 ± 0.08

**Table 8.10** Biodistribution of  $^{99m}\text{Tc}$ -labeled MPCL570 after intravenous injection in EAT bearing Balb/c mice. Radioactivity was counted in each organ and expressed as percent injected dose per gm of organ/tissue. Each value is the mean  $\pm$  S. D. of 5 mice.

Organs	% Injected dose per gram of tissue			
	1 h	2 h	4 h	24 h
Blood	3.47 ± 0.21	3.32 ± 0.35	3.11 ± 0.22	1.01 ± 0.19
Heart	0.85 ± 0.07	1.07 ± 0.08	0.47 ± 0.06	0.37 ± 0.10
Lung	2.50 ± 0.22	1.37 ± 0.16	1.01 ± 0.08	0.66 ± 0.11
Liver	13.59 ± 2.34	10.04 ± 2.01	8.32 ± 1.94	4.03 ± 0.34
Spleen	5.15 ± 0.24	4.55 ± 0.28	3.26 ± 0.30	1.63 ± 0.06
Kidney	3.02 ± 0.13	3.33 ± 0.19	2.92 ± 0.14	1.23 ± 0.05
Stomach	1.08 ± 0.09	0.71 ± 0.08	0.44 ± 0.04	0.39 ± 0.04
Intestine	0.46 ± 0.07	0.67 ± 0.10	0.85 ± 0.08	0.23 ± 0.04
Tumor	1.50 ± 0.35	2.24 ± 0.25	2.70 ± 0.61	1.23 ± 0.05

**Table 8.11** Biodistribution of  $^{99m}\text{Tc}$ -labeled YPCL570 after intravenous injection in EAT bearing Balb/c mice. Radioactivity was counted in each organ and expressed as percent injected dose per gm of organ/tissue. Each value is the mean  $\pm$  S. D. of 5 mice.

Organs	% Injected dose per gram of tissue			
	1 h	2 h	4 h	24 h
Blood	3.50 ± 0.23	3.38 ± 0.15	3.01 ± 0.20	1.04 ± 0.17
Heart	1.01 ± 0.05	0.97 ± 0.09	0.83 ± 0.14	0.18 ± 0.06
Lung	2.23 ± 0.24	1.71 ± 0.14	1.13 ± 0.05	0.79 ± 0.11
Liver	13.07 ± 1.23	10.34 ± 1.35	6.99 ± 1.35	3.95 ± 0.64
Spleen	4.79 ± 0.36	3.52 ± 0.24	2.71 ± 0.18	1.81 ± 0.33
Kidney	3.58 ± 0.25	3.45 ± 0.12	2.53 ± 0.34	1.11 ± 0.07
Stomach	0.88 ± 0.05	0.62 ± 0.07	0.40 ± 0.08	0.19 ± 0.08
Intestine	1.31 ± 0.21	0.95 ± 0.09	0.65 ± 0.16	0.55 ± 0.12
Tumor	1.78 ± 0.36	2.32 ± 0.21	2.43 ± 0.16	1.14 ± 0.09

**Table 8.12** Biodistribution of  $^{99m}\text{Tc}$ -labeled EPCL570 after intravenous injection in EAT bearing Balb/c mice. Radioactivity was counted in each organ and expressed as percent injected dose per gm of organ/tissue. Each value is the mean  $\pm$  S. D. of 5 mice.

The biodistribution profile of plain ETO and micellar formulations (peptide conjugated and non conjugated) are represented in Table 8.6 to 8.12 and was expressed as the percent injected dose per gram of tissue or organ (% ID/gm tissue/organ). Compared to plain ETO, micellar formulation exhibited a totally different distribution pattern. Moreover, the percent uptake and distribution was found different for different organs/tissues. In plain ETO after 1 h post injection, the blood concentration observed was almost 3 fold lower compared to micellar formulations and was reduced quickly to 0.29 % ID after 24 h. This implies that plain ETO eliminates quickly from body over a time. In contrast to this, all micellar formulation showed longer circulation with significant activity even after 24 h post injection (Figure 8.1). The MPCL235, YPCL235 and EPCL235 showed 5.75, 4.27 and 4.37 fold greater concentrations respectively in blood after 24 h compared to plain ETO. While, MPCL570, YPCL570 and EPCL570, the concentration was 3.93, 3.48 and 3.58 fold higher compared to plain ETO at 24 h post injection. A difference in blood concentration was also observed in MPCL570, YPCL570 & EPCL570 to MPCL235, YPCL235 & EPCL235. The probable reason behind these might be due to higher particle size of MPCL570, YPCL570 and EPCL570 micelles, which might resulted in to higher uptake by RES systems. The long circulating effect of micelles was attributed due to presence of PEG chain on the surface of micelles and was reported well by various authors due to stealth effect provided by PEG (Manosroi et al., 2003; Zhang et al., 2004; Forrest et al., 2008)

The largest contribution to total clearance occurred in the liver since it is the principal organ for drug metabolism. The liver uptake pattern of micellar formulations was totally different compared to plain ETO (Figure 8.2). In ETO, initially after 1 h post injection, liver showed  $7.96 \pm 1.68$  % ID and later on it reduced more quickly with  $2.87 \pm 0.17$  percent ID after 24 h post injection. All micellar formulations, after 1 h post injection exhibited near to two fold increase in liver uptake compared to plain ETO, in addition to this all micellar formulations demonstrated comparable liver uptake at all the time point. After 24 h post injection, the liver uptake of all micellar formulation was two fold higher compared to plain ETO and it indicates longer residence of micellar formulation in liver. Nevertheless, the liver uptake by micellar formulations was much lower compared to PLGA and PCL nanoparticles, which

showed two to three fold higher liver uptake (Snehalatha et al., 2008, Halder et al., 2008). The higher uptake of reports of PLGA and PCL nanoparticles by liver was attributed to larger particle size compared to micelles. In addition, micellar formulations showed higher liver uptake compared to plain ETO was due to their particulate drug delivery system with particle size smaller than 100 nm. It is assumed that micelles distributed mainly to parenchymal cells of the liver after intravenous injection and stayed longer time compared to plain drug (Stolnik et al., 2001). Therefore, these formulations can be used effectively in the treatment of liver carcinomas.

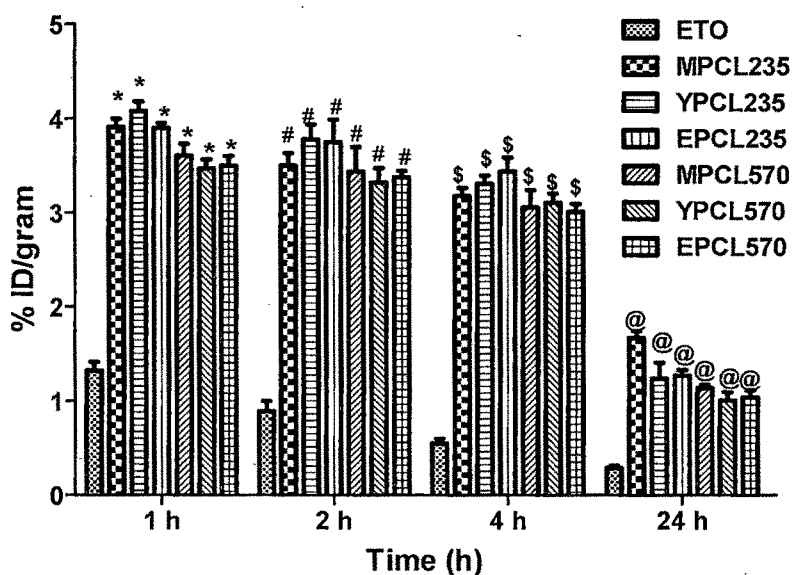


Figure 8.1 Biodistribution profile of  $^{99m}\text{Tc}$  labeled ETO and micellar formulations in blood of EAT tumor bearing mice after i.v. administration (n=5).

\*, #, \$ and @ indicates  $P < 0.001$  compared to ETO at 1, 2, 4 & 24 h respectively.

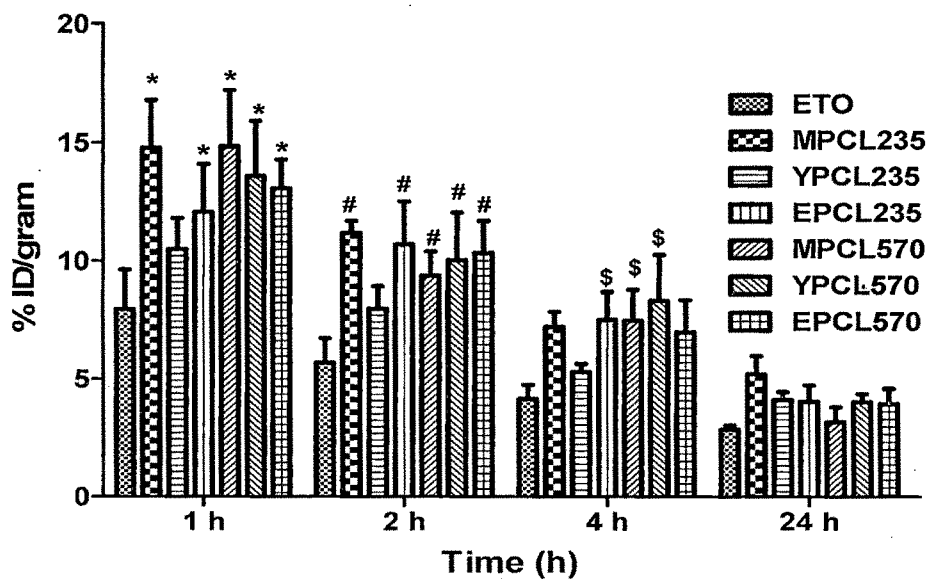


Figure 8.2 Biodistribution profile of <sup>99m</sup>Tc labeled ETO and micellar formulations in liver of EAT tumor bearing mice after i.v. administration (n=5). \*, # and \$ indicates P<0.001 with compared to ETO at 1, 2 & 4 h respectively.

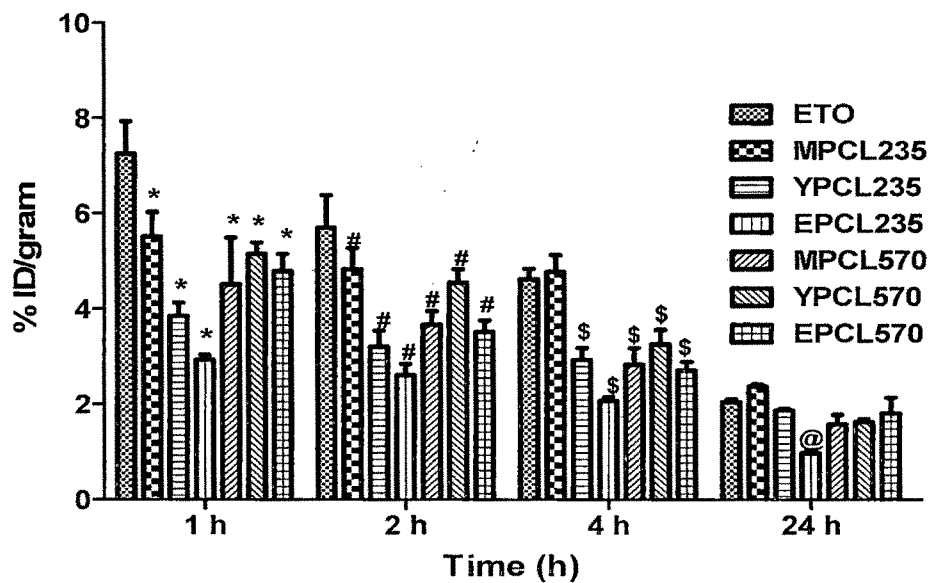


Figure 8.3 Biodistribution profile of <sup>99m</sup>Tc labeled ETO and micellar formulations in spleen of EAT tumor bearing mice after i.v. administration (n=5). \*, #, \$ and @ indicates P<0.001 compared to ETO at 1, 2, 4 & 24 h respectively.

Spleen is the second organ, where higher uptake of plain ETO and micellar formulation observed. However, the overall uptake of micellar formulations by spleen was found to lesser extent than plain ETO (Figure 8.3). The spleen uptake of MPCL235, YPCL235 & EPCL235 exhibited was  $5.52 \pm 0.51$ ,  $3.85 \pm 0.28$  &  $2.93 \pm 0.10$  percent respectively after 1 h post injection. At the same time point, MPCL570, YPCL570 & EPCL 570 exhibited spleen uptake of  $4.52 \pm 0.97$ ,  $5.15 \pm 0.24$  &  $4.79 \pm 0.36$  percent respectively. In both plain ETO and micellar formulation, the spleen uptake was decreased with increase in time. The splenic and liver uptake of micellar formulation was found higher due to the filtration effect these organs. According to Stolnik et al (1995), when particle size was greater than 200 nm, the accumulation of micelles in liver was higher and when the size was below 200 nm, the spleen was more powerful to catch the micelles because of its tighter structure. However, in present study, contrary results were observed and spleen showed lower uptake compared to liver. These could be due to smaller size of micelles below 100 nm which can penetrate more in liver compared to particle size of nanocarrier above 100 nm (Avgoustakis et al., 2003). Moreover, Zhang et al. (2004) has observed that camptothecin loaded PEG-PCL nanoparticles of particle size of 80 nm avoided spleen uptake more effectively than PEG-PCL nanoparticle of particle size about 180 nm.

The lung uptake of plain ETO and micellar formulation is represented in Figure 8.4. The plain ETO showed lung uptake of  $4.36 \pm 0.35$  percent at 1 h post injection, which was near to two fold higher compared to micellar formulations. All micellar formulation showed comparable lung activity and uptake at different time point. A lower lung uptake was observed in micellar formulation might be due to their smaller size, which helped in escaping of micelles from lungs (Zhang et al., 2004). A higher radioactivity in kidney was exhibited by plain ETO to that of micellar formulation (Figure 8.5). After 1 h post injection, the kidney uptake of plain ETO was  $6.63 \pm 2.36$  percent, while MPCL235, YPCL 235 and EPCL exhibited 1.93, 1.88 & 1.80 fold lower uptakes compared to plain ETO. MPCL570, YPCL570 and EPCL570 showed 2.46, 2.19 and 1.85 fold lower accumulations in kidney compared to plain ETO at same time point. The result obtained indicates slow excretion rate of micellar formulations and lower renal toxicity.

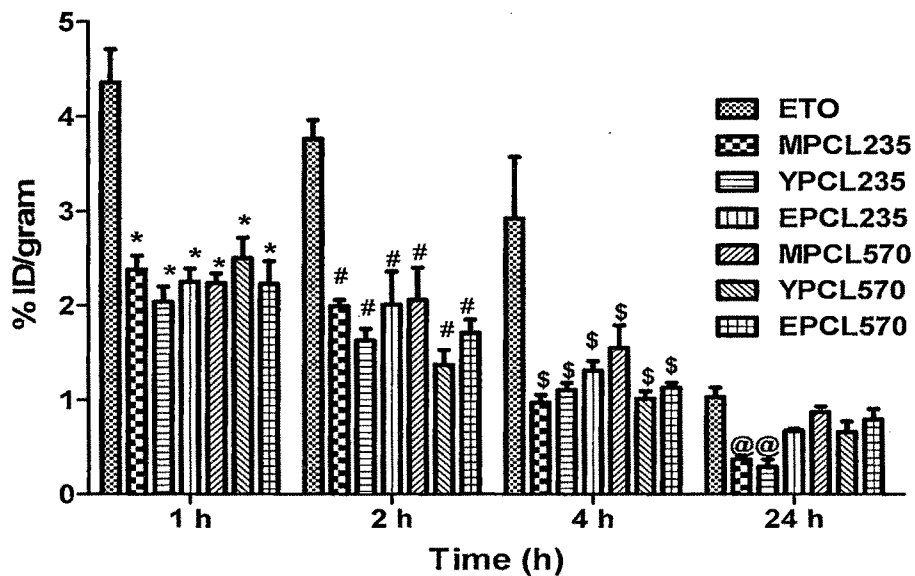


Figure 8.4 Biodistribution profile of  $^{99m}\text{Tc}$ -labeled ETO and micellar formulations in lung of EAT tumor bearing mice after i.v. administration (n=5). \*, #, \$ and @ indicates  $P < 0.001$  compared to ETO at 1, 2, 4 & 24 h respectively.

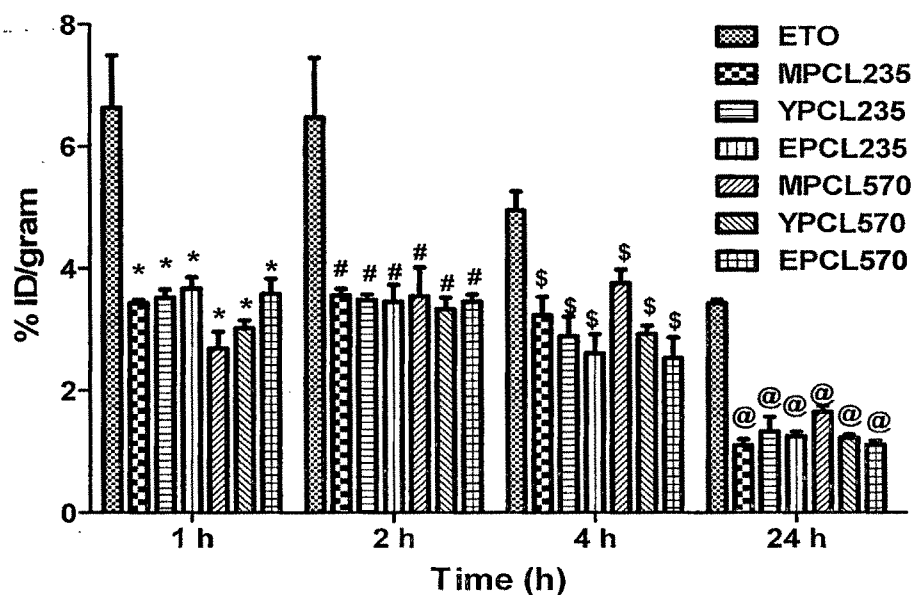


Figure 8.5 Biodistribution profile of  $^{99m}\text{Tc}$  labeled ETO and micellar formulations in kidney of EAT tumor bearing mice after i.v. administration (n=5). \*, #, \$ and @ indicates  $P < 0.001$  compared to ETO at 1, 2, 4 & 24 h respectively.

Radioactivity of micellar formulations in heart was lower compared to plain ETO after 1 h post injection, suggesting lower cardiac toxicity of micellar formulations (Figure 8.6). In all micellar formulations i.e. peptide conjugated and non conjugated, almost similar pattern of biodistribution was observed in organs like lung, liver, spleen, kidney, heart, stomach, intestine except blood. A minor difference in percent uptake by various organs was observed in peptide conjugated micelles to non conjugated micelles. However, the obtained data did not reflect the major differentiation in biodistribution study. The similarity in biodistribution pattern of peptide conjugated micelles to non conjugated micelles might be attributed to a low level of receptor expression in normal organ cells.

A prominent difference in tumor uptake of micellar formulation was observed compared to plain ETO (Figure 8.7). Plain ETO showed very poor tumor penetration and hence lower uptake at all the time point compared to micellar formulations. Plain ETO after 1 h post injection showed 0.38 percent tumor uptake and it reduced to 0.08 percent after 24 h post injection. The reduction in tumor uptake of plain ETO was observed as time lengthened while tumor uptake of micellar formulation increased upto certain time point. The stealth micelles i.e. MPCL235 and MPCL570 showed a 2.57 and 2.15 fold higher tumor uptake to plain ETO at 1 h post injection and exhibited maximum tumor uptake of  $1.78 \pm 0.10$  &  $1.92 \pm 0.38$  percent respectively after 4 h post injection (Figure 8.7). A higher tumor uptake was seen in MPCL235 and MPCL570, which was attributed to passive targeting by means of their smaller size (Shai et al., 2005). Peptide YIGSR-NH<sub>2</sub> conjugated micelles, YPCL235 and YPCL570 exhibited maximum tumor uptake of  $2.62 \pm 0.14$  &  $2.70 \pm 0.61$  percent respectively after 4 h post injection which was almost 12 to 13 fold higher compared to plain ETO (Figure 8.7). EILDV-NH<sub>2</sub> conjugated micelles, EPCL235 and EPCL570 showed the maximum tumor uptake of  $2.43 \pm 0.16$  &  $2.96 \pm 0.17$  percent at 4 h, which was 11.97 & 14.89 fold higher compared to plain ETO (Figure 8.7). These results suggest that the tumor uptake can be significantly increased by surface decoration of micelles with ligand which can interact with surface cell receptors and resulting into receptor mediated endocytosis. The findings obtained was in accordance of Hyaluronic acid conjugated PEG-PCL micelles which showed enhanced tumor uptake in EAT tumor induced mice (Yadav et al., 2008).

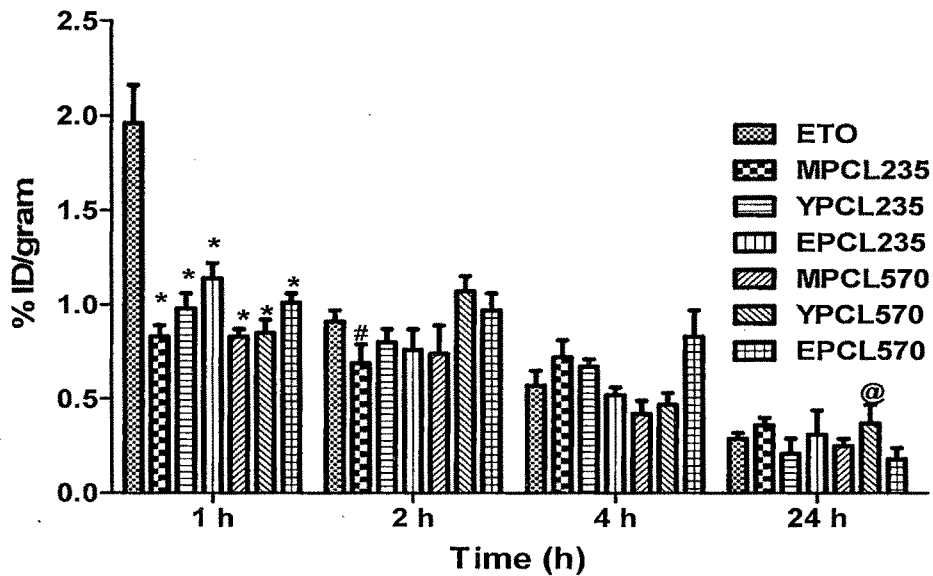


Figure 8.6 Biodistribution profile of  $^{99m}\text{Tc}$  labeled ETO and micellar formulations in heart of EAT tumor bearing mice after i.v. administration (n=5). \*, #, and @ indicates  $P < 0.001$  compared to ETO at 1, 2 & 24 h respectively.

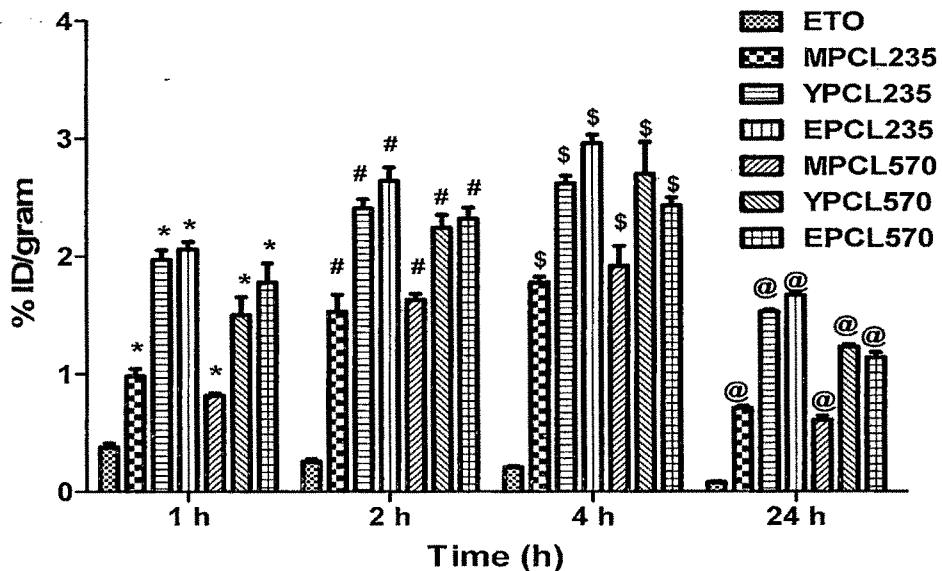


Figure 8.7 Biodistribution profile of  $^{99m}\text{Tc}$  labeled ETO and micellar formulations in tumor of EAT tumor bearing mice after i.v. administration (n=5). \*, #, \$ and @ indicates  $P < 0.001$  compared to ETO at 1, 2, 4 & 24 h respectively.

### 8.3.2 Experimental metastasis

Experimental metastasis study was conducted using highly metastatic B16F10 cells which were reported to produce pulmonary metastatic nodules in lungs after intravenous injection of cells (Gude et al., 1996; Cameron et al., 2000). In actual metastatic process which is observed in subcutaneously developed tumor, several processes such as primary invasion, transport into circulation, survival in circulation, arrest in the capillary bed of an organ, extravasation into the parenchyma and several other steps are involved. Compared to these, many of these steps are not seen in the experimental metastasis model. Although, this model is very useful in investigating the process of organ specificity of tumor cells involving homing to lung and the subsequent cell-cell interaction. As metastatic cells need to attach themselves to lung basement membrane before they grow into nodules, cell adhesion plays a vital part in the metastatic spreading of B16 melanoma (Gude et al., 1996).

It is also observed for many years that metastasis is inherently an inefficient process. In large number of experiments, in which tumor cells have been introduced directly in the circulation of mice or rats, around 0.01% of these cells form metastatic foci. Similarly, large numbers of cancer cells might be detected in the blood in cancer patients, and yet very few of these develop into overt metastases (Luzzi et al., 1998; Duchosal et al., 2001). The experimental metastasis study was conducted by two different methods to find out the potential of B16F10 cells for the induction of metastasis i.e. by pre-treatment and post-treatment method.

#### 8.3.2.1 *In vitro* treatment of B16F10 melanoma cells with formulations and its effect on inhibition of lung metastasis (Pre-treatment method)

In this study, B16F10 cells were treated with subtoxic concentration of ETO and ETO loaded micellar formulations (IC<sub>25</sub>, 48 h) and then injected to mice via tail vein to examine the effect formulations on inhibition of pulmonary metastatic nodules formation. The total number of nodules formation in untreated control group found was  $154.4 \pm 26.8$  and the percent inhibition in lung nodule formation calculated is represented Table 8.13 & Figure 8.8.

Formulations	Number of metastatic nodules	% Inhibition in pulmonary metastatic nodule formation
UC	154.4 ± 26.8	-----
ETO	80.4 ± 18.1	47.92 ± 11.78
MPCL235	69.6 ± 19.7	54.91 ± 12.77
YPCL235	33.2 ± 8.0	78.49 ± 5.22
EPCL235	24.8 ± 4.7	83.93 ± 3.05
MPCL570	63.6 ± 5.4	58.80 ± 3.50
YPCL570	27.4 ± 11.1	82.24 ± 7.19
EPCL570	19.2 ± 4.1	87.55 ± 2.68

Table 8.13 Effect of *in vitro* ETO and ETO loaded micelles treated B16F10 cells on inhibition of nodule formation in C57BL/6 mice (Pre-treatment). The results are mean ± S.D. and n= 5 animals.

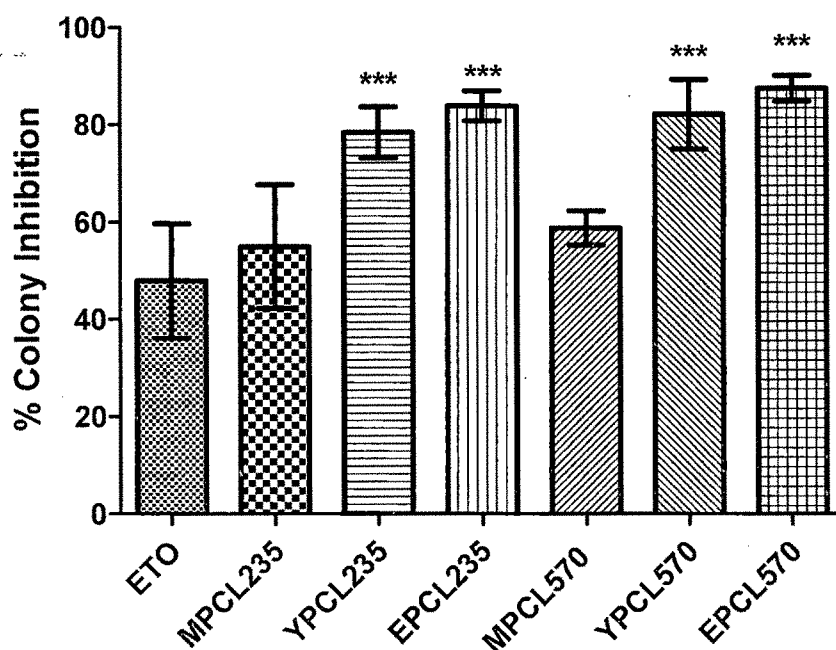
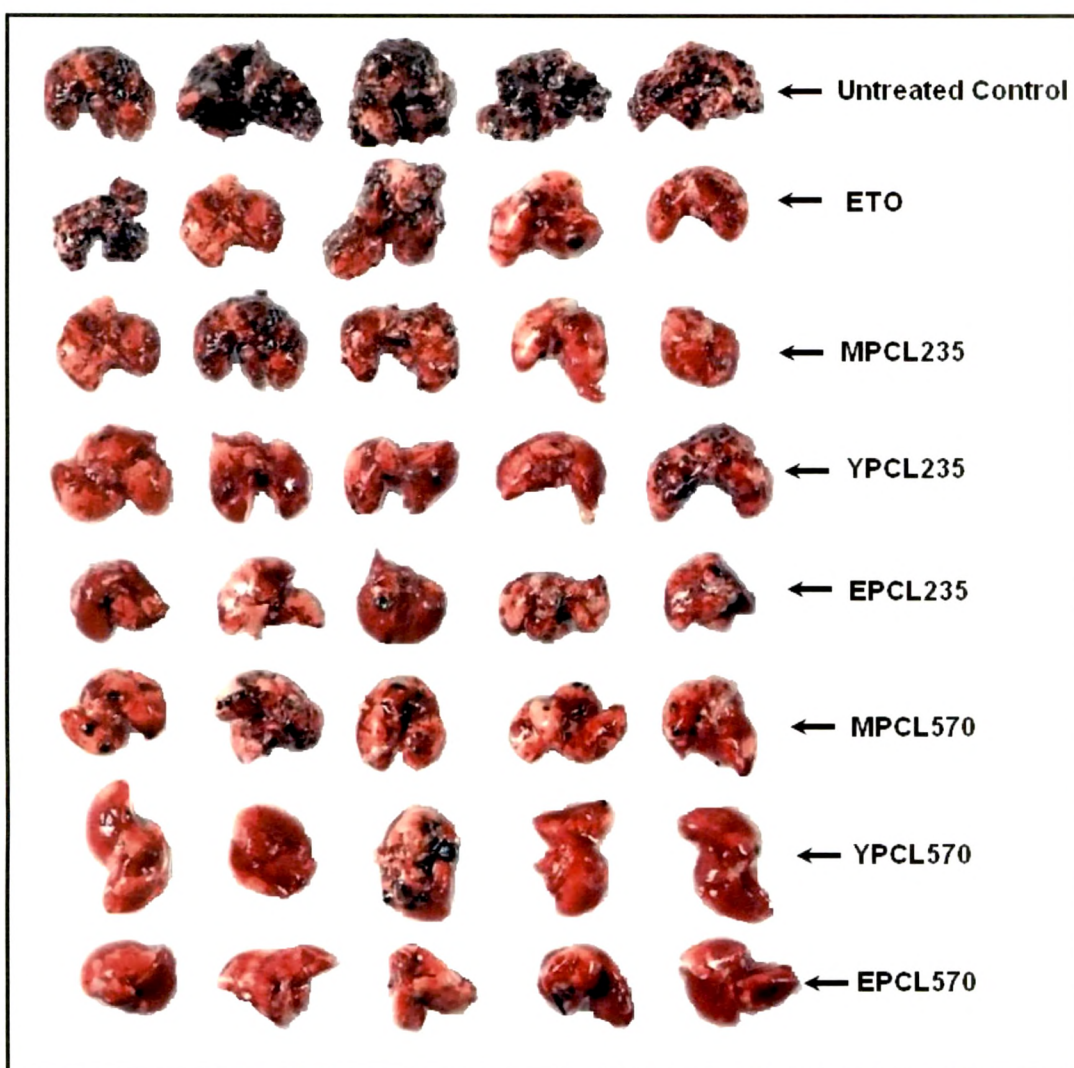


Figure 8.8 Effect of *in vitro* ETO and ETO loaded micelles treated B16F10 cells on inhibition of nodule formation in C57BL/6 mice (Pre-treatment). (\*\*\*) represents  $P < 0.001$  compared to ETO)

The *in vitro* treated B16F10 cells with plain ETO and ETO loaded micellar formulations exhibited reduction in formation of pulmonary metastatic nodules with maximum effect seen in peptide conjugated micelles with  $P < 0.001$ . Compared to plain ETO which showed  $47.92 \pm 11.78$  percent inhibitions in metastatic nodules, micellar formulation showed higher inhibition (Table 8.13). The possible reason attributed to this might be due to intracellular uptake and controlled release of drug over a longer period of time. MPCL235, YPCL235 and EPCL235 micellar formulations showed  $54.91 \pm 12.77$ ,  $78.49 \pm 5.22$  &  $83.93 \pm 3.05$  percent inhibition in pulmonary metastatic nodules formation respectively while MPCL570, YPCL570 and EPCL570 showed  $58.80 \pm 3.50$ ,  $82.24 \pm 7.19$  &  $87.55 \pm 2.68$  percent inhibition respectively. The results obtained implies that ETO and ETO loaded micellar formulations might have interacted directly or indirectly with tumor cell (B16F10 cell) surface receptors involved in adhesion to lung basement membrane (Gude et al., 1996). It is also assumed that after *in vitro* incubation of B16F10 cells with ETO and ETO loaded micellar formulations, the change in morphology of B16F10 cells observed in cytopathic study might be affected the adhesion of B16F10 cells to lung basement membrane. Peptide tagged micelles as compared to non conjugated micelles showed near to 1.5 fold higher efficacies in prevention of metastasis, which might be due to higher intracellular uptake as well altered receptor configuration required for adhesion to lung membrane. This method has an advantage that it represents the identical situation, where the cancer affected patient receiving anticancer drug therapy and during this treatment, metastasis is under process. Figure 8.9 shows the lung images, in which it is clearly seen that as compared to untreated control, B16F10 cells treated with ETO and ETO loaded micellar formulations groups have lesser number of metastatic nodules formation which appeared as black spot in figure.



**Figure 8.9** Appearance of lungs after 21<sup>st</sup> day of *in vitro* treated B16F10 cells inoculation (Pre-treatment).

### 8.3.2.2 *In vivo* treatment of B16F10 melanoma and its effect on inhibition of lung metastasis with formulations (Post-treatment)

In post-treatment method, ETO and ETO loaded micellar formulations were injected by intravenous route on second day of B16F10 cells inoculation to C57BL/6 mice. After 21<sup>st</sup> day of cell inoculation, the numbers of pulmonary metastatic nodules were counted and the results obtained are represented in Table. 8.14 & Figure 8.10. It was observed that all formulations showed their potential towards inhibition in metastatic nodule formations

Formulations	Number of metastatic nodules	% Inhibition in pulmonary metastatic nodule formation
Untreated control	152.6 ±31.3	-----
ETO	96.8 ±11.7	36.72 ± 7.85
MPCL 235	78.4 ±15.2	48.60 ± 10.04
YPCL 235	52.2 ±7.8	65.77 ± 5.16
EPCL 235	57.0 ±17.5	62.64 ± 11.52
MPCL 570	70.2 ±8.9	53.99 ± 9.42
YPCL 570	54.2 ±12.7	64.47 ± 8.33
EPCL 570	46.4 ±6.4	69.58 ± 4.23

Table 8.14 Effect of intravenous treatment of ETO and ETO loaded micellar formulations on inhibition of pulmonary metastatic nodule formation of B16F10 cells inoculated C57BL/6 mice (Post-treatment). The results are mean ± S.D. and the n= 5 animals.

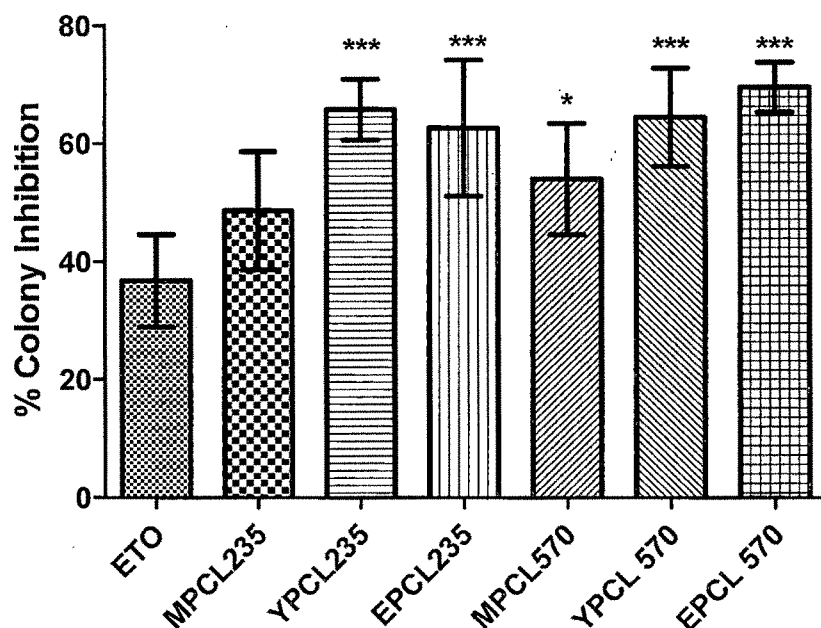


Figure 8.10 Effect of intravenous treatment of ETO and ETO loaded micellar formulations on inhibition of pulmonary metastatic nodule formation of B16F10 cells inoculated mice (Post-treatment). (\*\*\*) and \* represents  $P < 0.001$  and  $P < 0.05$  compared to ETO)

The plain ETO showed  $36.72 \pm 7.85$  percent inhibitions in nodule formation while MPCL235, YPCL235 and EPCL235 showed  $48.60 \pm 10.04$ ,  $65.77 \pm 5.16$  &  $62.64 \pm 11.52$  percent inhibitions in metastatic pulmonary nodules formation respectively. Similarly, MPCL570, YPCL570 and EPCL570 showed  $53.99 \pm 9.42$ ,  $64.47 \pm 8.33$  &  $69.58 \pm 4.23$  percent inhibitions in lung nodule formation respectively. Peptide (YIGSR-NH<sub>2</sub>/EILDV-NH<sub>2</sub>) conjugated micelles compared to plain ETO and non conjugated micelles showed near to 1.75 and 1.40 fold higher inhibitions in metastatic nodules formation respectively. The results obtained signifies the worth potential of peptide conjugated micellar drug delivery for effective prevention and treatment of metastasis. The higher inhibition observed in YIGSR-NH<sub>2</sub> and EILDV-NH<sub>2</sub> conjugated micelles was assumed to be due to its interactions with surface cell receptor present on B16F10 cells circulating in blood stream. Since, before adhesion to secondary site like lung for metastasis, the tumor cell circulates in body and interacts with various components present in blood including any drug carrier. However, deep investigations are still necessary to prove the interactions of nanocarrier with tumor cells circulating in blood. This method represents the identical situation where cancer detected in secondary stage in which metastasis has already been in progress.

Pentoxifylline loaded liposomes exhibited higher antimetastatic activity compared to plain pentoxifylline solution and showed the usefulness of nanocarrier in treatment of metastasis as reported earlier (Sant et al., 2000). Moreover, Jantscheff et al. (2009) reported that gemcitabine liposomal formulation was potentially efficient in prevention of metastasis using LNCaP prostate cancer xenograft model. The market available DOXIL<sup>®</sup> (pegylated doxorubicin liposomes) which is used in metastasis was not that much defined by clinical trials due to poor understanding of its role in prevention of metastasis. It is believed that the antimetastasis effect was rather due to inhibition in growth of primary tumor (Zhang et al., 2008). They also suggested that for complete eradication of pulmonary metastasis, surgical removal of primary tumor plus multiple injections of pegylated doxorubicin liposomes are needed. In this situation, antimetastatic peptide like YIGSR-NH<sub>2</sub> and EILDV-NH<sub>2</sub> which can recognize and adhere on the surface of circulating tumor cell detached from primary tumor. Peptide conjugated micellar formulations might be useful in such

circumstances and able to internalize into tumor cell and interferes with metastasis cascade. Earlier reports with niosomal cisplatin at dose of 1mg/kg showed percent inhibition in lung nodule formation near to 71.91 percent compared to free cisplatin (38.47 %) using B16F10 cell line (Gude et al., 2002). However it is required to mention that the efficacy of different anticancer drug will vary based on dose. The appearance of lungs after metastatic melanoma nodules formations can be seen in Figure 8.11.

Pre-treatment method exhibited higher inhibition in pulmonary metastatic nodule formation compared to post-treatment method. However, it is difficult to correlate each other due to difference in treatment and dose of drug given by intravenous route.

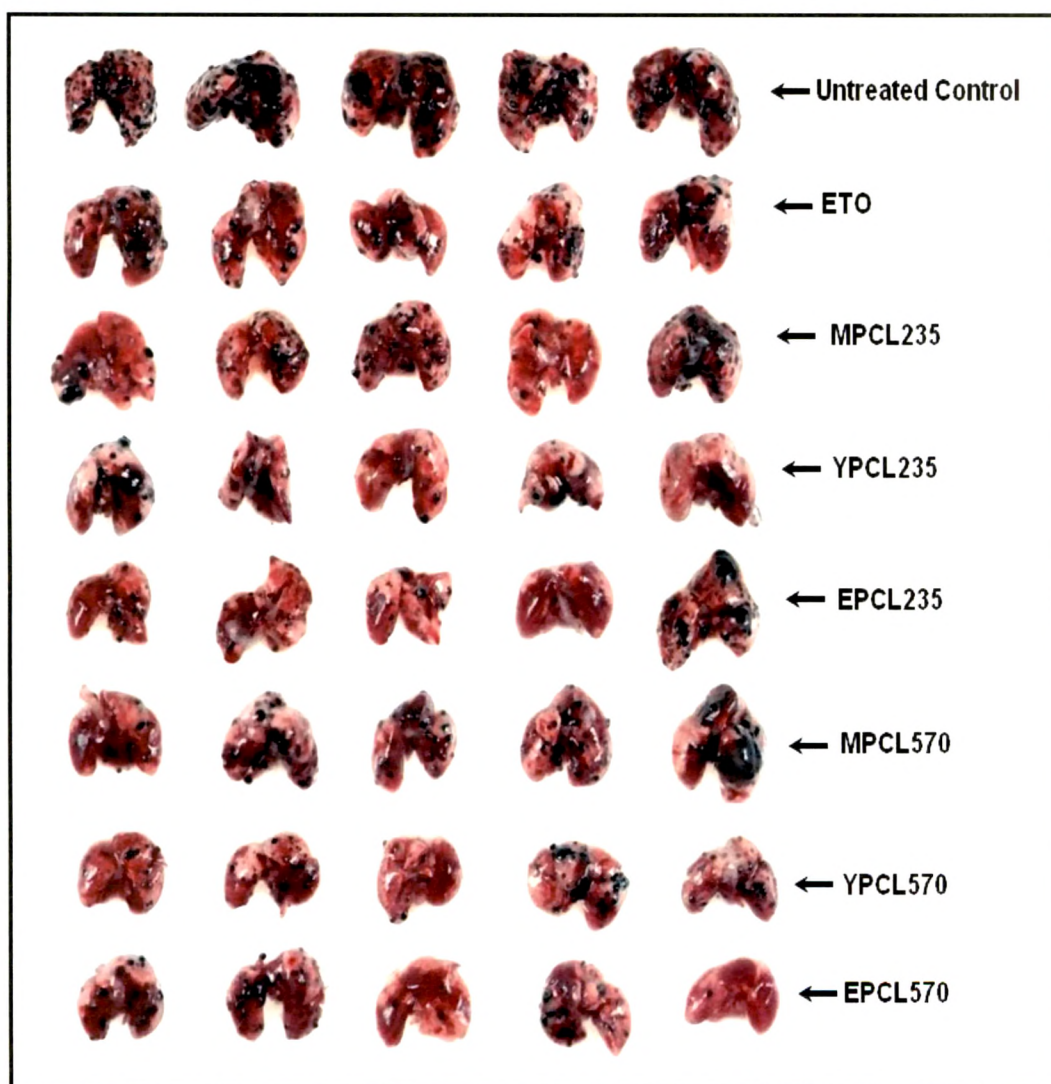


**Figure 8.11 Appearance of lungs after 21<sup>st</sup> day of B16F10 cells inoculations followed by intravenous treatment of formulations (Post-treatment).**

### 8.3.2.1 Histopathology studies

Histopathology studies were carried out in both the groups i.e. pre-treatment and post-treatment experimental metastasis model to examine any changes in the nature of metastatic pattern of lung. The lung of untreated group was considered as control.

In pretreatment model, the histological examinations are shown in Figure 8.12. The untreated control exhibited small to large size tumor islands which covered entire lung parenchyma and also blocked the lumen of medium and large blood vessels. Moreover, tumor cells penetrated the middle coat of blood vessels and lodged in several blood vessels. In case of ETO, smaller size of tumor islands with lesser extent of multiplicity was observed compared to control. MPCL235 and MPCL570 treated groups showed reduction in number of tumor islands with smaller size compared to control. A greater extent of reduction in size as well as number of tumor islands was observed in peptide tagged formulations. Compared to YPCL235 & YPCL570, a smaller size of tumor islands was observed in EPCL235 and EPCL570. In addition to this, the blood vessels were found unblocked in peptide conjugated micelles treated groups.

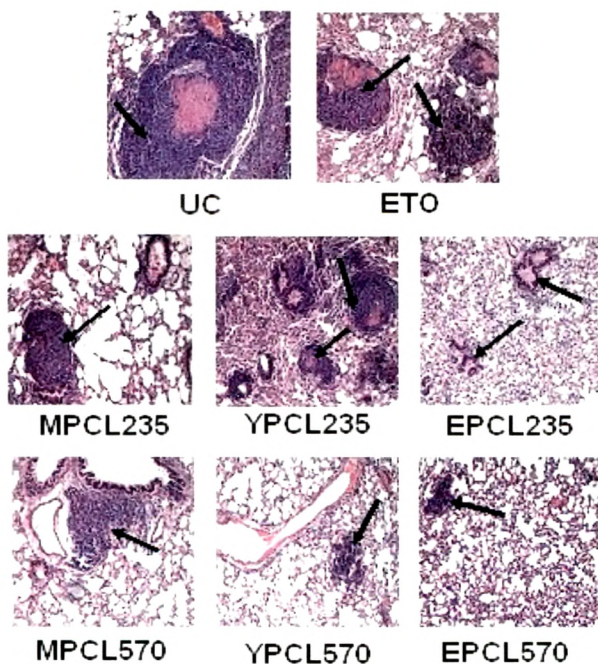


**Figure 8.12** Histopathological studies of lung tissues showing reduction in tumor islands by *in vitro* treated B16F10 cells with various formulations (Pre treatment).

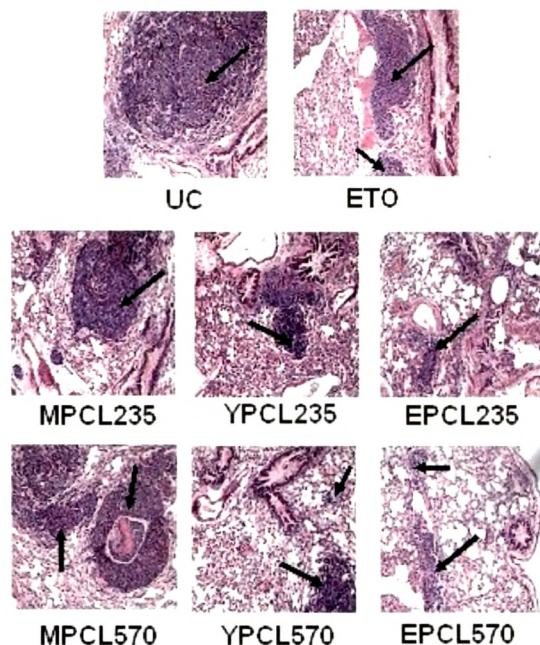


**Figure 8.13** Histopathological studies of lung tissues showing reduction in tumor islands by *in vivo* treatment with various formulations (Post-treatment).

In post treatment method, similar findings were seen but the size of tumor islands in all formulations was larger to some extent compared to pretreatment method (Figure 8.13). Peptide conjugated micellar formulations showed reduction in tumor island size and numbers identical to non conjugated micelles and plain ETO.

## REFERENCES

- Avgoustakis K, Belestsi A, Panagi Z, Klepetsanis P, Livaniou E, Evangelatos G, Ithakissios DS. Effect of copolymer composition on the physicochemical characteristics, in vitro stability and biodistribution of PLGA-mPEG nanoparticles. *Int J Pharm* 2003; 259:115-127.
- Babbar A, Kashyap R, Chauhan UP. A convenient method for the preparation of <sup>99m</sup>Tc-labelled pentavalent DMSA and its evaluation as a tumour imaging agent. *J Nucl Biol Med* 1991; 35:100-104.
- Cameron DM, Schmidt EE, Kerkvliet N, Nadkarni KV, Morris VL, Groom AC, Chambers AF, MacDonald IC. Temporal progression of metastasis in lung: cell survival, dormancy, and location dependence of metastatic inefficiency. *Cancer Res* 2000; 60: 2541-2546.
- Duchosal MA, Mauray S, Ruegg M, Trouillet P, Vallet V, Aarden L, Tissot JD, Schapira M. Human peripheral blood leukocyte engraftment into SCID mice: critical role of CD4(+) T cells. *Cell Immunol* 2001; 211: 8-20.
- Forrest ML, Yanez JA, Rembsberg CM, Ohgami Y, Kwon GS, Davies NM. Paclitaxel prodrugs with sustained release and high solubility in poly(ethylene glycol)-b-poly(ε-caprolactone) micelle nanocarriers: Pharmacokinetic disposition, tolerability and cytotoxicity. *Pharm Res* 2008; 25: 194-206.
- Gude RP, Binda MM, Hceter LP, Andres K, Daniel RB. Studies on the mechanisms responsible for inhibition of experimental metastasis of B16-F10 murine melanoma by pentoxifyline. *J Biomed Sci* 1999; 6: 133-141.
- Gude RP, Ingle AD, Rao SGA. Inhibition of lung homing of B16F10 by pentoxifylline, a microfilament depolymerizing agent. *Cancer Lett* 1996; 106: 171-176.
- Gude RP, Jadhav MG, Rao SGA, Jagtap AG. Effects of niosomal cisplatin and combination of the same with theophylline and with activated macrophages in murine B16F10 melanoma model. *Cancer Biother Radiopharm* 2002; 17: 183-192.
- Halder KK, Mandal B, Debnath MC, Bera H, Ghosh LK, Gupta BK. Chloramphenicol incorporated polylactide-co-glycolide (PLGA) nanoparticles: Formulation, characterization, technetium-99m labeling and biodistribution studies. *J Drug Target* 2008; 16: 311-320.

Jantscheff P, Zirolli V, Esser N, Graeser R, Kluth J, Sukolinskaya A, Taylor LA, Unger C, Massing Y. Anti-metastatic effects of liposomal gemcitabine in a human orthotopic LNCaP prostate cancer xenograft model. *Clin Exp Metastasis* 2009; 26: 981–992.

Luzzi, KJ, MacDonald IC, Schmidt EE, Kerkvliet N, Morris VL, Chambers AF, Groom AC. Multistep nature of metastatic inefficiency: dormancy of solitary cells after successful extravasation and limited survival of early micrometastases. *Am J Pathol* 1998; 153: 865-873.

Manosroi A, Wongtrakul P, Manosroi J, Sakai H, Sugawara F, Yuasa M, Abe M. Characterization of vesicles prepared with various non-ionic surfactants mixed with cholesterol. *Coll Surf B Biointerf* 2003; 30:129-138.

Mishra P, Babbar A, Chauhan UP. A rapid instant thin layer chromatographic procedure for determining radiochemical purity of <sup>99</sup>Tcm-IDA agents. *Nucl Med Commun* 1991; 12: 467–469.

Ratheesh A, Ingle A, Gude RP. Pentoxifylline modulates cell surface integrin expression and integrin mediated adhesion of B16F10 cells to extracellular matrix components. *Cancer Biol Ther* 2007; 6: 1743-1752.

Reddy LH, Sharma RK, Chuttani K, Mishra AK, Murthy RSR. Influence of administration route on tumor uptake and biodistribution of etoposide loaded solid lipid nanoparticles in Dalton's lymphoma tumor bearing mice. *J Control Release* 2005; 105: 185–198.

Sant VP, Nagarsenkar MS, Rao SGA, Gude RP. Enhancement of anti-metastatic Activity of pentoxifylline by encapsulation in conventional liposomes and sterically stabilized liposomes in murine experimental B16F10 melanoma model. *J Pharm Pharmacol* 2000; 52: 1461-1466.

Shai B, Fang C, You MX, Zhang Y, Fu S, Pei YY. Stealth MePEG-PCL micelles: effects of polymer composition on micelle physicochemical characteristics, in vitro drug release, in vivo pharmacokinetics in rats and biodistribution in S180 tumor bearing mice. *Colloid Polym Sci* 2005; 283: 954–967.

Snehalatha M, Venugopal K, Saha RN, Babbar AK, Sharma RK. Etoposide loaded PLGA and PCL nanoparticles II: biodistribution and pharmacokinetics after radiolabeling with Tc-99m. *Drug Deliv* 2008; 15: 277-287.

Stolnik S, Heald CR, Neal J, Garnett MC, Davis SS, Illum L, Purkis SC, Barlow RJ, Gellert PR. Polylactide-poly(ethylene glycol) micellar-like particles as potential drug carriers: Production, colloidal properties and biological performance. *J Drug Target* 2001; 9: 361–378.

Stolnik S, Illum L, Davis SS. Long circulating microparticulate drug carriers. *Adv Drug Deliv Rev* 1995; 16: 195-214.

Taylor A, Jr, Akiya, F, Gregory MC. Failure to visualize acutely injured kidneys with Technetium-99m DMSA does not preclude recoverable function. *J Nucl Med* 1986; 27: 377-379.

Theobald AE.. Quality control of radiopharmaceuticals. In: *Textbook of Radiopharmacy: Theory and Practice*, Sampson, C. B. (Ed.) New York: Gordon and Breach Science. 1990; 127-129.

Yadav A, Mishra P, Jain S, Mishra P, Mishra AK, Agrawal GP. Preparation and characterization of HA-PEG-PCL intelligent core-corona nanoparticles for delivery of doxorubicin. *J Drug Target* 2008; 16: 464-478.

Zhang L, Hu Y, Jiang X, Yang C, Lu W, Yang YH. Camptothecin derivative-loaded poly(caprolactone-co-lactide)-b-PEG-b-poly(caprolactone-co-lactide) nanoparticles and their biodistribution in mice. *J Control Release* 2004; 96: 135-148.

Zhang Y, Li A, Wang Z, Han Z, He J, Ma J. Antimetastatic activities of pegylated liposomal doxorubicin in a murine metastatic lung cancer model. *J Drug Target* 2008; 16: 679-687.